Ubiquitin S65 phosphorylation engenders a pH-sensitive conformational switch

Xu Dong (董旭)[a,b,1], Zhou Gong (龚洲)[a,b,1], Yun-Bi Lu (卢韵碧)[c], Kan Liu[a,b], Ling-Yun Qin[a,b], Meng-Lin Ran[a,b], Chang-Li Zhang[d], Zhu Liu (刘主)[c,2], Wei-Ping Zhang (张纬萍)[c,e,2], and Chun Tang (唐淳)[a,b,f,g,2]

[a]Key Laboratory of Magnetic Resonance in Biological Systems of the Chinese Academy of Sciences, State Key Laboratory of Magnetic Resonance and Atomic Molecular Physics, Wuhan Institute of Physics and Mathematics of the Chinese Academy of Sciences, Wuhan, Hubei Province 430071, China; [b]National Center for Magnetic Resonance at Wuhan, Wuhan Institute of Physics and Mathematics of the Chinese Academy of Sciences, Wuhan, Hubei Province 430071, China; [c]Department of Pharmacology, Institute of Neuroscience, Key Laboratory of Medical Neurobiology of the Ministry of Health of China, Zhejiang University School of Medicine, Hangzhou, Zhejiang Province 310058, China; [d]Guilin Medical University, Guilin, Guangxi Province 541004, China; [e]Zhejiang Province Key Laboratory of Mental Disorder's Management, Zhejiang University School of Medicine, Hangzhou, Zhejiang Province 310058, China; [f]Wuhan National Laboratory for Optoelectronics, Wuhan, Hubei Province 430074, China; and [g]Collaborative Innovation Center of Chemistry for Life Sciences, Wuhan Institute of Physics and Mathematics of the Chinese Academy of Sciences, Wuhan, Hubei Province 430071, China

Edited by Michael F. Summers, Howard Hughes Medical Institute, University of Maryland, Baltimore County, Baltimore, MD, and approved May 23, 2017 (received for review April 6, 2017)

Ubiquitin (Ub) is an important signaling protein. Recent studies have shown that Ub can be enzymatically phosphorylated at S65, and that the resulting pUb exhibits two conformational states—a relaxed state and a retracted state. However, crystallization efforts have yielded only the structure for the relaxed state, which was found similar to that of unmodified Ub. Here we present the solution structures of pUb in both states obtained through refinement against state-specific NMR restraints. We show that the retracted state differs from the relaxed state by the retraction of the last β-strand and by the extension of the second α-helix. Further, we show that at 7.2, the pK_a value for the phosphoryl group in the relaxed state is higher by 1.4 units than that in the retracted state. Consequently, pUb exists in equilibrium between protonated and deprotonated forms and between retracted and relaxed states, with protonated/relaxed species enriched at slightly acidic pH and deprotonated/retracted species enriched at slightly basic pH. The heterogeneity of pUb explains the inability of phosphomimetic mutants to fully mimic pUb. The pH-sensitive conformational switch is likely preserved for polyubiquitin, as single-molecule FRET data indicate that pH change leads to quaternary rearrangement of a phosphorylated K63-linked diubiquitin. Because cellular pH varies among compartments and changes upon pathophysiological insults, our finding suggests that pH and Ub phosphorylation confer additional target specificities and enable an additional layer of modulation for Ub signals.

ubiquitin | phosphorylation | protein dynamics | pH sensitivity | conformational switch

Ubiquitin (Ub), a 76-residue signaling protein, is found ubiquitously in cells. Two or more Ub molecules can be covalently linked to form a diubiquitin (diUb) and then a polyubiquitin (polyUb), as an isopeptide bond is formed between the carboxylate group of one Ub (called the distal Ub) and the amine group of another Ub (called the proximal Ub). Owing to the characteristic quaternary structures of polyUb and specific interactions between polyUb and its target proteins (1, 2), a polyUb with a specific linkage can be involved in a distinctive set of cellular functions (3).

The heterogeneity of Ub also arises from other types of covalent modifications. Proteomics studies have indicated that Ub is phosphorylated at multiple sites (4, 5). However, PINK1 is the only Ub kinase known to date, which specifically phosphorylates Ub at S65 (6, 7). Under normal conditions, only a fraction of Ub is S65-phosphorylated. However, upon oxidative stress, neurodegeneration, or aging, the level of S65 phosphorylation increases significantly (4, 8). S65-phosphorylated Ub (pUb) in turn can activate PARKIN, a ubiquitin ligase, and induce mitophagy (9–12). However, no other pUb-specific targets have been clearly identified, and how phosphorylation affects Ub signaling in general remains unclear.

Previously, Komander and coworkers showed that pUb gives two distinct sets of NMR peaks, which correspond to the two conformational states of pUb exchanging at a slow timescale (13). Based on NMR long-range HNCO experiments, the authors concluded that the two states differ in the hydrogen-bonding network involving the last β-strand (β5)—the β5 moves up by two residues and the C-terminal tail in one conformational state is then retracted. However, crystallization efforts yielded only the structure for the relaxed state, which turned out to be similar to the structure of unphosphorylated wild-type Ub (13, 14). Furthermore, S65D or S65E phosphomimetic mutants of pUb afforded only a single set of NMR peaks (13) and failed to fully mimic S65 phosphorylation (4).

The various organelles and compartments inside a cell are buffered at specific pHs (15). Because Ub is involved in myriad aspects of cellular processes, it is possible that pH may play a role in Ub function. Acids are continuously generated from metabolic activities. Therefore, the homeostasis of cellular pH has to be maintained, and slight pH change, even transient and localized, can serve as a cellular signal (15, 16). For example, the loss of pH gradient across the inner membrane of mitochondria often

Significance

Ubiquitination and phosphorylation are the two most important protein posttranslational modifications and cell signals. Ubiquitin can be specifically phosphorylated at S65, and the finding here suggests a general functional role for Ub phosphorylation. We show that subtle fluctuation near physiological pH can affect the protonation status of the S65 phosphoryl group and modulate the structure of the ubiquitin monomer and polyubiquitin. It is known that cellular pH varies among organelles and changes under physiological and pathological conditions. Because ubiquitin is involved in myriad aspects of cell biology, a pH-sensitive conformational switch acquired upon S65 phosphorylation would allow phosphorylated ubiquitin to interact with different target proteins upon environmental cues. It would also enable cross-talk between ubiquitination and phosphorylation signals.

Author contributions: X.D., Y.-B.L., Z.L., W.-P.Z., and C.T. designed research; X.D., Z.G., L.-Y.Q., M.-L.R., C.-L.Z., and Z.L. performed research; X.D., Z.G., K.L., Z.L., W.-P.Z., and C.T. analyzed data; and X.D., Z.G., Y.-B.L., Z.L., W.-P.Z., and C.T. wrote the paper.

The authors declare no conflict of interest.

This article is a PNAS Direct Submission.

Data deposition: The atomic coordinates for the pUb retracted state and relaxed state have been deposited in the Protein Data Bank, www.pdb.org (PDB ID codes 5XK4 and 5XK5, respectively), and the associated NMR chemical shifts and restraints have been deposited in the BioMagResBank, www.bmrb.wisc.edu (accession nos. 36081 and 36082, respectively).

[1]X.D. and Z.G. contributed equally to this work.

[2]To whom correspondence may be addressed. Email: liuzhu@wipm.ac.cn, weiping601@zju.edu.cn, or tanglab@wipm.ac.cn.

This article contains supporting information online at www.pnas.org/lookup/suppl/doi:10.1073/pnas.1705718114/-/DCSupplemental.

preludes mitophagy (17), a process involving PARKIN and pUb. Therefore, we hypothesize that pH may regulate the function of pUb during mitophagy as well as other cellular processes.

To understand how S65 phosphorylation and pH may impact Ub signals, we set out to determine the solution structures of pUb in both relaxed and retracted states. We came to discover that the S65 phosphoryl group in the relaxed state has an unusually elevated pK_a value, much higher than that in the retracted state. As a result, the pUb interconverts between relaxed and retracted states and also between protonated and deprotonated species, whose equilibrium is shifted in response to slight pH change. Using phosphorylated K63-linked diubiquitin (pK63-diUb) as a reporter, we further show that the pH-dependent conformational switch of pUb can be translated into the rearrangement of Ub subunits in pK63-diUb. Thus, we propose that S65 phosphorylation modulates the structure of polyUb and enables polyUb to interact with different target proteins.

Results and Discussion

The Solution Structure of pUb Relaxed and Retracted States. We identified 125 peaks for the backbone amide of pUb in the ^{1}H-^{15}N heteronuclear single-quantum coherence (HSQC) spectrum (Fig. S1). Among these peaks, 59 can be assigned to the relaxed state, 56 can be assigned to the retracted state, and 10 can be assigned to both states. Starting from well-resolved peaks, we could make nearly complete assignment of side-chain resonances and obtain state-specific NOE distance restraints (Fig. S2) and residual dipolar coupling (RDC) restraints. For the 10 overlapped residues, only intraresidue or sequential NOE restraints were applied and no RDC restraints. Refining against the different types of restraints, we determined the solution structures of pUb in both relaxed and retracted states (Table S1).

The structure for the relaxed state is well-converged, with a root-mean-square (RMS) deviation of 0.24 ± 0.05 Å for backbone heavy atoms (Fig. 1*A* and Fig. S3). The relaxed state structure is similar to the crystal structures of pUb previously determined (Fig. S4 *A* and *B*) (13, 14), with RMS differences of <0.8 Å for backbone heavy atoms. The solution structure for the relaxed state is also similar to the structure of unphosphorylated Ub, with backbone RMS differences of <0.8 Å (Fig. S4 *C* and *D*) (18, 19).

The structure for the retracted state also converges well, with a backbone RMS deviation of 0.33 ± 0.07 Å (Fig. 1*B*, Fig. S5, and Table S1). To assess the accuracy of the structure, we performed multiple cross-validations. Leaving out one set of RDC restraints, we could still obtain the structure of the retracted state, which is similar to the structure obtained by refining against the full set of restraints (Fig. S6 *A* and *B*). Significantly, the free RDC restraints can be cross-validated with the working structures (Fig. S6 *C* and *D*). We also refined the structure of the retracted state with a subset of randomly selected NOE distance restraints. Regardless, the calculations afforded similar structures (Fig. S6 *E* and *F*). It means that the NOEs are self-consistent, and unlikely to arise from a different conformational state of pUb.

Structural comparison reveals the difference between the two states of pUb. As previously shown (13), the strand β5 moves up by two residues in the retracted state. The β5 in the retracted state

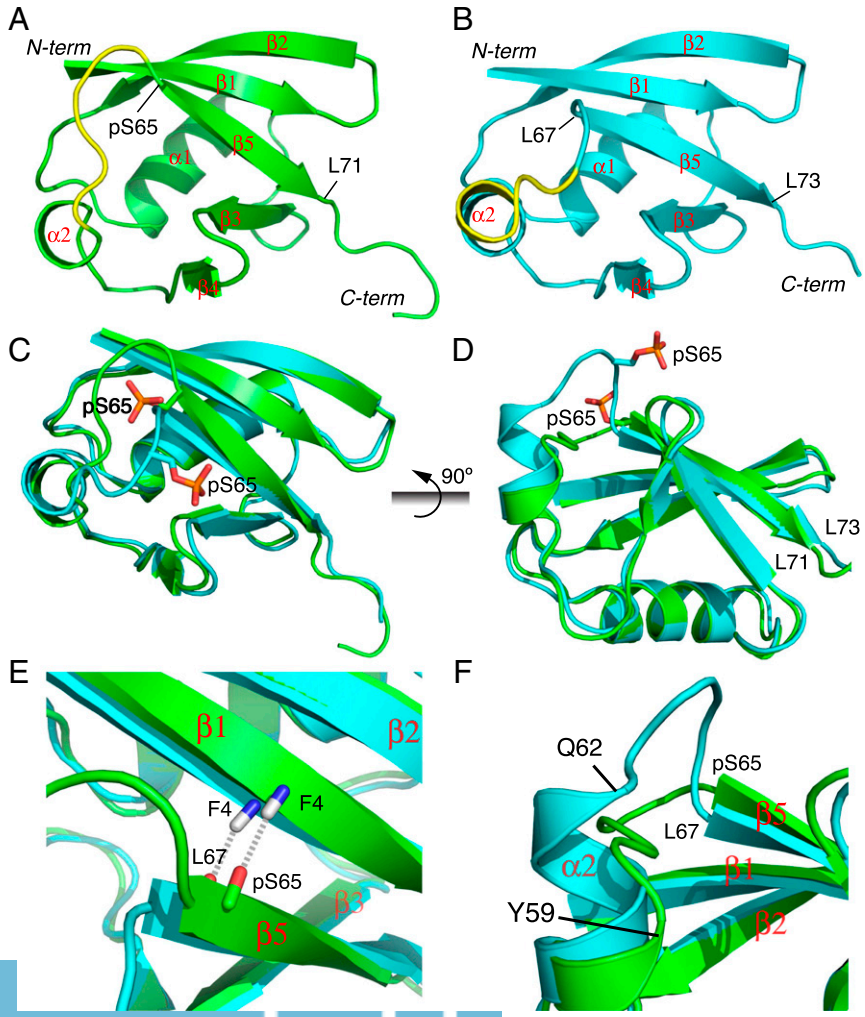

Fig. 1. Solution structures of pUb. (*A*) Structure of pUb in the relaxed state. (*B*) Structure of pUb in the retracted state. The structure shown is closest to the mean, with the secondary structures labeled and α2-β5 loop (residues 60 to 64) highlighted. (*C* and *D*) Comparison between the two conformational states of pUb in different perspectives. The backbone RMS difference between the two is 0.79 Å for residues 1 to 58. The last residues in β5 are labeled. (*E*) Close-up view of strand β5. The amide group of F4, indicated with dashed lines, is hydrogen-bonded to L67 in the retracted state and to pS65 in the relaxed state. (*F*) Close-up view of helix α2. α2 extends by three residues to Q62 in the retracted state instead of Y59 in the relaxed state.

comprises residues L67 to L73, and the backbone carbonyl group of L67 forms an interstrand hydrogen bond with the amide group of F4 (Fig. 1 *C* and *E*). In the relaxed state, β5 comprises residues pS65 to L71, with the carbonyl group of pS65 hydrogen-bonded to the amide group of F4. In addition to β5 retraction, helix α2 extends by three more residues in the retracted state ending at Q62, as opposed to Y59 in the relaxed state (Fig. 1 *D* and *F*). Accompanying the secondary structure changes, the residues in the loop connecting α2 and β5 undergo a large movement, as large as ~10 Å, between the two conformational states (Fig. 1 *A* and *B*).

pH Regulates the Abundance of the Two pUb States. At pH 7.4, we found that the well-resolved peaks for the two conformational states of pUb have nearly the same peak intensities. However, in the previous NMR study done at a slightly lower pH, it was found that the relaxed state of pUb had a larger population (13). To assess whether the difference in the relative peak intensities arises from different buffer conditions, we collected ^{1}H-^{15}N HSQC spectra of pUb at pH values of 7.4, 6.9, 6.4, and 5.9. As the pH decreases, the peak intensities for the retracted state decrease, whereas the peak intensities for the same residues in the relaxed state increase (Fig. 2 *A* and *C*).

The peak intensities of all pUb residues follow the same trend in response to pH, but details vary. At pH 7.4, the relative peak intensities between retracted state and relaxed state can be >1 for some residues but much smaller for some others. For example, the peak intensity of Q62 in the retracted state is 2.21 times that in the relaxed state, whereas the peak intensity of L69 in the retracted state is only 0.59 times that in the relaxed state (Fig. 2*E*). The deviations likely arise from structural change and local dynamics. Thus, the peak intensities measured from 2D ^{1}H-^{15}N HSQC spectra may not reflect the exact populations of the two states.

S65 Phosphoryl Group in the Relaxed State Has an Unusually High pK_a. To understand what triggers the interconversion between the two states, we collected a series of 1D ^{31}P spectra over a broad range of pH from 4 to 9. Unlike 2D ^{1}H-^{15}N HSQC spectra, we could easily integrate the volume for each ^{31}P peak, which corresponds to the exact population of the associated conformational state. At pH 7.4, two ^{31}P peaks can be observed, and the integral for the downfield peak is slightly larger than the integral for the upfield peak (Fig. 3*A*). As pH decreases, the integral for the upfield peak increases and reaches ~80% of the total pUb; as pH increases, the integral for the downfield ^{31}P increases and reaches ~60% of the total pUb (Fig. 3*B*). The change in volumes of the two ^{31}P peaks in response to pH is in good agreement with the pattern identified from 2D ^{1}H-^{15}N HSQC spectra. Therefore, the upfield ^{31}P peak should be from the relaxed state, whereas the downfield ^{31}P peak should be from the retracted state.

The ^{31}P chemical shift is also an ideal indicator for the protonation status of the phosphoryl group, which can differ by up to 4 ppm between deprotonated (dianionic) and protonated (monoanionic) species (20, 21). Both ^{31}P peaks of pUb shift progressively upon pH change, and we could fit the pK_a values of 5.83 ± 0.02 and 7.21 ± 0.03 for the retracted state and relaxed state, respectively (Fig. 3*C*). The pK_a value for the retracted state is consistent with the value generally observed for the serine phosphoryl group (21), and is also consistent with the structure of the retracted state in

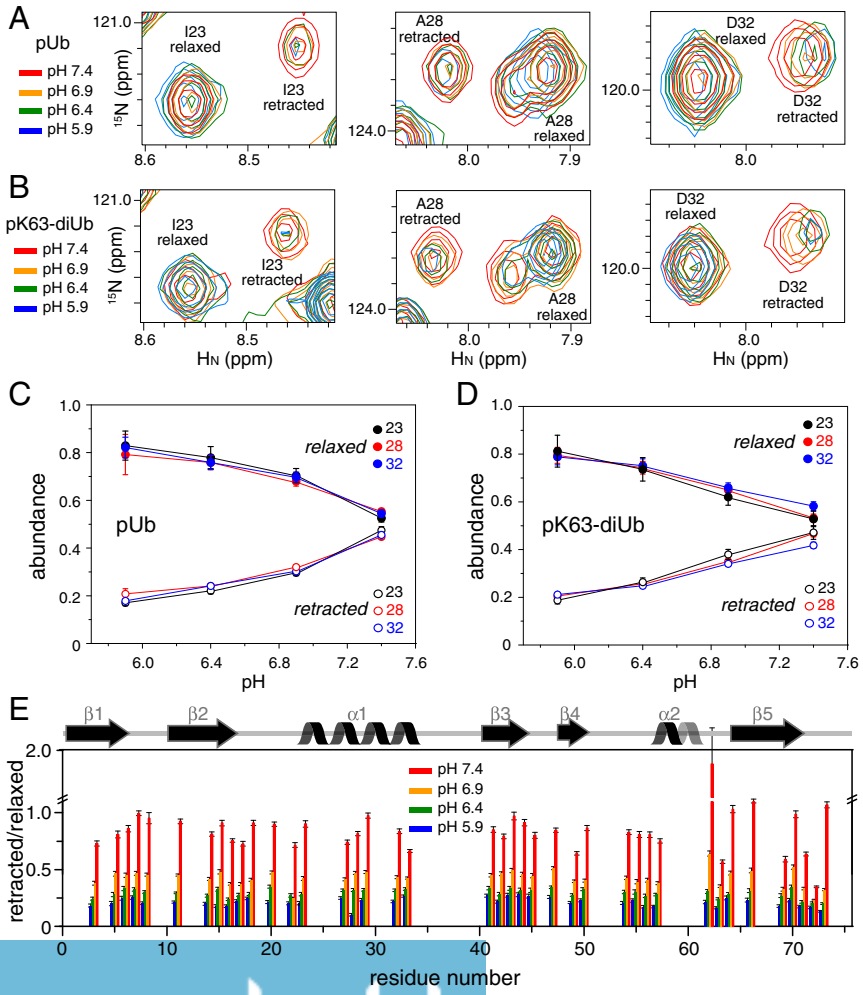

Fig. 2. Changes of NMR peak intensities in response to pH. (*A* and *B*) Overlay of ^{15}N-HSQC spectra for residues I23, A28, and D32 in pUb and the proximal Ub of pK63-diUb, respectively. The data were collected at 298 K with the proteins prepared in 20 mM Pipes buffer containing 150 mM NaCl. These residues are far from pS65, and experience relatively little chemical-shift perturbations upon pH change. (*C* and *D*) The abundance of the relaxed or retracted state, roughly proportional to the peak intensities, is plotted as a function of pH. (*E*) Relative peak intensity for all of the residues in pUb. Only the peaks that can be quantified for both states in all pH conditions are shown. Error bars indicate the SD propagated from the peak-intensity measurements. The secondary structures of pUb are indicated.

which pS65 is located in a loop and its side chain is solvent-exposed (Fig. 1*D*). However, the pK_a value for the relaxed state is unusually elevated, differing from that of the retracted state by 1.4 pH units.

To explain why the pK_a value of pS65 in the relaxed state is so elevated, we performed molecular dynamics (MD) simulations for the different species of pUb. As indicated by backbone RMS fluctuations, the protonated/relaxed species is more stable than deprotonated/relaxed species of pUb, whereas the deprotonated/retracted species is more stable than protonated/retracted species of pUb (Fig. S7). Importantly, the simulations revealed that the protonated S65 phosphoryl group in the relaxed state could form a hydrogen bond with the backbone carbonyl group of K63 in an ideal geometry (Fig. 3*D*). This hydrogen bond would stabilize the protonated/relaxed species of pUb and account for the unusually high pK_a value.

Based on the pK_a values and based on the relative abundance of the two pUb states at various pHs, we determined the equilibrium constants for the interconversion between the relaxed state and retracted state, which are 15.2 ± 1.1 from the protonated/retracted species to the protonated/relaxed species and 1.7 ± 0.1 from the deprotonated/relaxed species to the deprotonated/retracted species (Fig. 3*E*). As such, the coupled equilibria explain why the protonated/relaxed species is enriched at slight acidic pH and the deprotonated/retracted species is enriched at slightly basic pH.

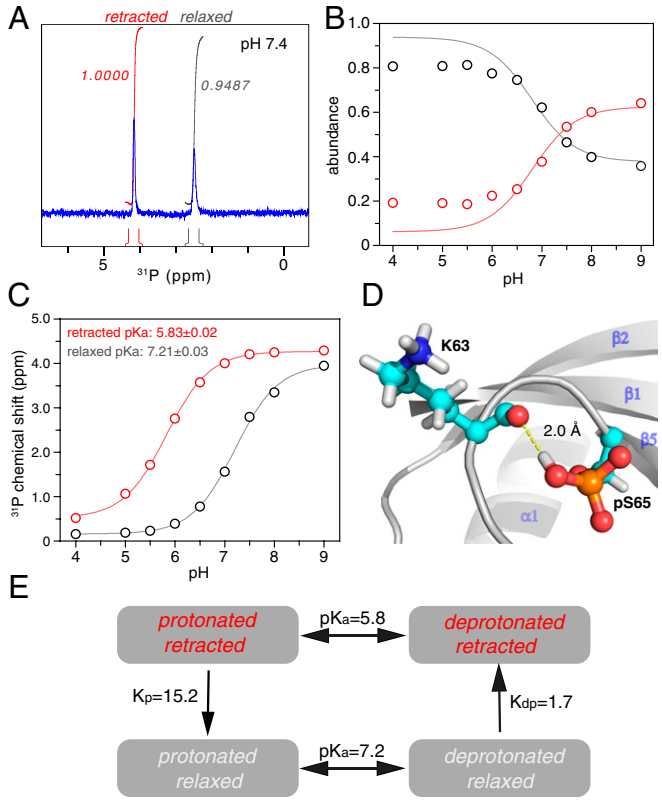

Fig. 3. pUb exists in equilibrium among four chemical species. (*A*) Two ^{31}P peaks can be observed with about the same integrated peak volumes, which can be assigned to the pS65 phosphoryl group in the retracted state and relaxed state. (*B*) The relative abundance of the two conformational states, quantitated by ^{31}P peak integrals, changes in response to pH. (*C*) The ^{31}P chemical-shift value changes in response to pH. The pK_a values can be fitted for the retracted state and relaxed state. (*D*) The unusually high pK_a value for the relaxed state can be attributed to a hydrogen bond between the protonated pS65 phosphoryl group and the backbone carbonyl of K63. (*E*) Illustration of the coupled equilibriums of pUb, with the equilibrium constants denoted. A slight decrease in pH leads to the enrichment of protonated/relaxed species of pUb, whereas a slight increase in pH leads to the enrichment of deprotonated/retracted species of pUb.

Using these four equilibrium constants, we could also backcalculate the populations for the relaxed and retracted states, which agree well with the experimental values at pH between 6.5 and 8 (Fig. 3*B*). At more acidic pH, however, the experimental population for the retracted state hovers at ~0.2, higher than the calculated value. It is possible that additional factors such as protonation of neighboring E64 may help to stabilize the retracted state at acidic pH.

Ub Phosphomimetic Mutants Are Similar to Wild Type. Glutamate or aspartate substitution of serine is commonly used for mimicking phosphorylated serine, as it can be easily engineered. However, a previous NMR study showed that the mutant has only one set of NMR peaks (13). Here we collected the backbone RDC values for Ub S65E and S65D mutants and assessed them against the structures of the relaxed state of pUb and unmodified wild-type Ub (Fig. S8). The good correlations between the observed and calculated RDCs indicate that the structures of phosphomimetic mutants are similar to the structure of the relaxed state. On the other hand, the RDC values measured for the phosphomimetic mutants agree poorly with the structure of the retracted state, with the largest discrepancies observed for residues in β5 and the α2-β5 loop (Figs. S8 and S9).

We also compared the electrostatic potentials of the various structures (Fig. S10). The electrostatic surface of the S65E or S65D mutant appears similar to that of the protonated/relaxed species of pUb. However, pUb can carry two negative charges at residue 65 either in its relaxed state or retracted state, which would have drastically different electrostatic surfaces. Hence, the different charge states and conformational heterogeneity of pUb explain why glutamate or aspartate substitution poorly mimics Ub S65 phosphorylation.

pH Modulates Quaternary Structures of Phosphorylated Diubiquitin. Because polyUb is the predominant form in cells (22), we asked whether the structure and dynamics of phosphorylated polyUb are also affected by pH. K63 is close to the phosphorylation site, and moves by ~10 Å between the two conformational states of pUb. Thus, the quaternary structures of K63-linked diubiquitin (K63-diUb) may be affected by S65 phosphorylation. With an unlabeled pUb attached at K63 of an ^{15}N-labeled pUb, we evaluated the peak intensities of proximal pUb in response to pH. Just like the pUb monomer, the peak intensities of the relaxed state in pK63-diUb also decrease when the pH increases, and at pH 7.4 have nearly the same intensities as the corresponding peaks in the retracted state (Fig. 2 *B* and *D*). Because the relative abundance of the two states is dictated by the equilibrium shift among the four pUb species (Fig. 3*E*), it can be reasoned that the proximal pUb in pK63-diUb has the same pH-sensitive conformational switch as the pUb monomer does.

We have shown previously that K63-diUb adopts three interconverting conformational states, each responsible for recognizing a specific target protein (2). Also in that study, we showed that the two closed states of K63-diUb, namely C1 and C2, are populated at a 3:1 ratio in the absence of a target protein. Here, using single-molecule fluorescence resonance energy transfer (smFRET) with fluorophores conjugated at the N25C site of distal Ub and G76C site of proximal Ub, we directly visualized the conformational distribution of K63-diUb. The single-molecule measurement allows a straightforward assessment of the constituting conformational states in a dynamic system without the complication from ensemble averaging (23, 24). At pH 7.4, we found that the smFRET profile of K63-diUb can be fitted as the sum of three Gaussian functions (Figs. S11–S13). Centering at FRET efficiencies of about 24, 47, and 64%, the populations for the low-, medium-, and high-FRET species are 10, 23, and 67%, respectively (Fig. 4*A*). The high-FRET and medium-FRET species have a ratio of 3:1, suggesting that these two species correspond to the two closed states previously characterized (2). When the pH is dropped to 6.4, the smFRET profile for K63-diUb remains the same (Fig. 4*C*), indicating that the structure of unphosphorylated K63-diUb is insensitive to pH.

Using the same labeling scheme, we characterized the conformational space of pK63-diUb. Its smFRET profile can also be fitted as the sum of three FRET species, which center at the same FRET efficiencies as those observed for K63-diUb. However, the population for the high-FRET species is only 54% at pH 7.4, whereas the population for the medium-FRET species is 35% for pK63-diUb (Fig. 4*B*). As the pH decreases to 6.4, the smFRET profile can still be fitted to three Gaussian functions (Fig. S13). However, more than 20% of the protein is converted from the medium-FRET species to the high-FRET species, with the latter populated at 79% (Fig. 4*D*).

Determination of the ensemble structures of pK63-diUb would be complicated, as it involves a permutation of the two conformational states for each Ub subunit. Thus, we modeled the structures based on the known ensemble structures of K63-diUb (2). Randomizing the configurations of the fluorophores attached to the C1 and C2 closed-state structures, we obtained interdye distances of 50.4 ± 9.7 and 56.1 ± 9.2 Å, respectively. The distances are in good agreement with the distances computed based on the FRET efficiencies, 47.4 and 53.2 Å for high- and medium-FRET species, respectively. Thus, the pH-sensitive movement of the α2-β5 loop and residue K63 in pUb may be piggybacked onto the domain movement of K63-diUb—the proximal pUb in the relaxed state appears compatible with the C1 closed state (Fig. 4*E*), and the proximal pUb in the retracted state appears compatible with the C2 closed state (Fig. 4*F*). This would explain why a pH decrease leads to the conversion from the medium-FRET species to the high-FRET species of pK63-diUb. Because the quaternary arrangement between Ub subunits is responsible for target specificity (1, 2), S65 phosphorylation would allow polyUb to interact with target proteins differently at different pHs.

Concluding Remarks

With the joint use of multiple biophysical techniques, we show here that the structure of pUb exists in equilibrium between protonated and deprotonated species and between retracted and relaxed states. Thanks to a hydrogen bond between the protonated phosphoryl group and the backbone carbonyl of K63, the S65 phosphoryl group in the relaxed state has an elevated pK_a value of 7.2. Consequently, any pH change can cause a shift of the equilibrium, enriching protonated/relaxed species or deprotonated/retracted species. pH-sensitive conformational switches have been reported for many other proteins (25–27). It has also been reported that K48-linked diubiquitin switches from a closed conformation to a predominant open conformation at pH 4.5 (28, 29). However, these examples of acid–base equilibrium all involve protein titratable side chains. Thus it is particularly interesting that a phosphoryl group can respond to subtle fluctuation around physiological pH and trigger a protein conformational switch.

The pH-sensitive conformational switch of the pUb monomer leads to the structural rearrangement of phosphorylated polyUb. The different quaternary structures of a polyUb would then confer upon the polyUb additional target specificities (1, 2). It is well-known that the different cell compartments are homeostatic at specific pHs. For example, the pH is ∼7.2 in the cytosol and nucleus, ∼8 inside mitochondria, between 6.0 and 6.7 in the Golgi, and more acidic in endosomes, ranging from 5.5 to 6.5 (15). Thus, the pH sensitivity may allow polyUb to perform location-specific functions. Moreover, the kinase of pUb, PINK1, is either anchored at mitochondria or exists as a soluble form in the cytosol (30). Thus, phosphorylated polyUb can be either recruited or generated on-site. Upon oxidative stress, neurodegeneration, and aging, Ub phosphorylation level drastically increases (4, 8, 31), whereas mitophagy, apoptosis, ischemia, inflammation, aging, and many pathophysiological conditions are all associated with changes in cellular pH (32–35). Altogether, it is likely that certain functions of pUb are only turned on in response to changes in both Ub phosphorylation level and environmental pH. Our finding thus opens a door for the better understanding of how phosphorylation regulates ubiquitin signaling.

Materials and Methods

Full methods are provided in *SI Materials and Methods*. Proteins were prepared following established protocols (13, 36, 37). NMR data collection was performed with Bruker 500-, 600- or 850-MHz spectrometers. The solution structures for the two states of pUb were refined using Xplor-NIH (38). Proteins labeled with Alexa Fluor 488 and Cy5 dyes were analyzed using a confocal microscope equipped with picosecond-pulsed lasers using an interleaved pulsing scheme

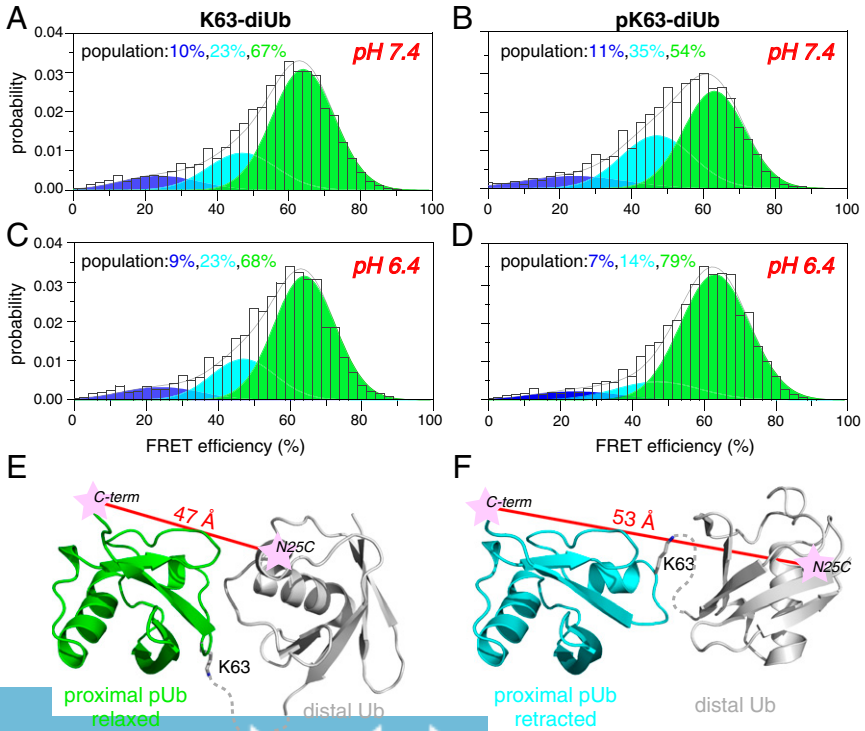

Fig. 4. Quaternary structure of pK63-diUb is pH-sensitive. (*A* and *C*) The smFRET profile of K63-diUb can be fitted as the sum of three FRET species. Centering at efficiencies of 24.3 ± 1.5, 47.4 ± 0.6, and 63.8 ± 0.6%, the populations for the three species are 10.0 ± 0.5, 22.7 ± 1.0, and 67.3 ± 1.4% at pH 7.4, and 9.2 ± 0.4, 23.2 ± 0.9, and 67.6 ± 0.7% at pH 6.4. (*B* and *D*) The smFRET profile of pK63-diUb can also be fitted as the sum of three FRET species. The populations for the three species are 10.9 ± 0.8, 34.1 ± 0.4, and 55.0 ± 0.7% at pH 7.4, and 6.8 ± 1.6, 14.0 ± 2.3, and 79.2 ± 1.4% at pH 6.4. (*E* and *F*) Structural models for the high- and medium-FRET species of pK63-diUb. Providing that the pH-sensitive movement of the α2-β5 loop is piggybacked onto the intrinsic subunit movement of K63-diUb, the FRET distance (indicated by red lines) is shorter when the proximal Ub is in the relaxed state (green cartoon) than it is in the retracted state (cyan cartoon). The Ub linkage is indicated with dashed lines.

(39). MD simulations were performed using AMBER 14 with the established parameters for phosphoserine (40).

ACKNOWLEDGMENTS. We thank Prof. Xin-Sheng Zhao for advice on smFRET data collection, and Chao Huang at ETSC Technologies and Chun-Yuan Zhou and Hong-Yi Chen at Nikon China for help with instrumentation. Grant support from the Chinese Ministry of Science and Technology (2013CB910200 to C.T. and W.-P.Z.; 2016YFA0501200 to C.T., Z.G., and X.D.), National Natural Science Foundation of China (31225007 to C.T.; 81573400 to W.-P.Z.; 31500595 to Z.L.; 31400735 to Z.G.; 31400644 to X.D.), and K.C. Wong Education Foundation made this research possible. Z.L. was supported in part by China Postdoctoral Science Foundation Grants 2015M571860 and 2016T90537. The research of C.T. was supported in part by an International Early Career Scientist grant from the Howard Hughes Medical Institute.

1. Ye Y, et al. (2012) Ubiquitin chain conformation regulates recognition and activity of interacting proteins. *Nature* 492:266–270.
2. Liu Z, et al. (2015) Lys63-linked ubiquitin chain adopts multiple conformational states for specific target recognition. *eLife* 4:e05767.
3. Yau R, Rape M (2016) The increasing complexity of the ubiquitin code. *Nat Cell Biol* 18:579–586.
4. Herhaus L, Dikic I (2015) Expanding the ubiquitin code through post-translational modification. *EMBO Rep* 16:1071–1083.
5. Swatek KN, Komander D (2016) Ubiquitin modifications. *Cell Res* 26:399–422.
6. Koyano F, et al. (2014) Ubiquitin is phosphorylated by PINK1 to activate parkin. *Nature* 510:162–166.
7. Kane LA, et al. (2014) PINK1 phosphorylates ubiquitin to activate Parkin E3 ubiquitin ligase activity. *J Cell Biol* 205:143–153.
8. Swaney DL, Rodríguez-Mias RA, Villén J (2015) Phosphorylation of ubiquitin at Ser65 affects its polymerization, targets, and proteome-wide turnover. *EMBO Rep* 16:1131–1144.
9. Wauer T, Simicek M, Schubert A, Komander D (2015) Mechanism of phospho-ubiquitin-induced PARKIN activation. *Nature* 524:370–374.
10. Sauvé V, et al. (2015) A Ubl/ubiquitin switch in the activation of Parkin. *EMBO J* 34: 2492–2505.
11. Lazarou M, et al. (2015) The ubiquitin kinase PINK1 recruits autophagy receptors to induce mitophagy. *Nature* 524:309–314.
12. Kumar A, et al. (2017) Parkin-phosphoubiquitin complex reveals cryptic ubiquitin-binding site required for RBR ligase activity. *Nat Struct Mol Biol* 24:475–483.
13. Wauer T, et al. (2015) Ubiquitin Ser65 phosphorylation affects ubiquitin structure, chain assembly and hydrolysis. *EMBO J* 34:307–325.
14. Han C, Pao KC, Kazlauskaite A, Muqit MM, Virdee S (2015) A versatile strategy for the semisynthetic production of Ser65 phosphorylated ubiquitin and its biochemical and structural characterisation. *ChemBioChem* 16:1574–1579.
15. Casey JR, Grinstein S, Orlowski J (2010) Sensors and regulators of intracellular pH. *Nat Rev Mol Cell Biol* 11:50–61.
16. Dechant R, et al. (2010) Cytosolic pH is a second messenger for glucose and regulates the PKA pathway through V-ATPase. *EMBO J* 29:2515–2526.
17. Wang Y, Nartiss Y, Steipe B, McQuibban GA, Kim PK (2012) ROS-induced mitochondrial depolarization initiates PARK2/PARKIN-dependent mitochondrial degradation by autophagy. *Autophagy* 8:1462–1476.
18. Vijay-Kumar S, Bugg CE, Cook WJ (1987) Structure of ubiquitin refined at 1.8 Å resolution. *J Mol Biol* 194:531–544.
19. Cornilescu G, Marquardt JL, Ottiger M, Bax A (1998) Validation of protein structure from anisotropic carbonyl chemical shifts in a dilute liquid crystalline phase. *J Am Chem Soc* 120:6836–6837.
20. Bienkiewicz EA, Lumb KJ (1999) Random-coil chemical shifts of phosphorylated amino acids. *J Biomol NMR* 15:203–206.
21. Platzer G, Okon M, McIntosh LP (2014) pH-dependent random coil (1)H, (13)C, and (15)N chemical shifts of the ionizable amino acids: A guide for protein pK_a measurements. *J Biomol NMR* 60:109–129.
22. Xu P, et al. (2009) Quantitative proteomics reveals the function of unconventional ubiquitin chains in proteasomal degradation. *Cell* 137:133–145.
23. Schuler B (2013) Single-molecule FRET of protein structure and dynamics—A primer. *J Nanobiotechnology* 11(Suppl 1):S2.
24. Deniz AA (2016) Deciphering complexity in molecular biophysics with single-molecule resolution. *J Mol Biol* 428:301–307.
25. Schnell JR, Chou JJ (2008) Structure and mechanism of the M2 proton channel of influenza A virus. *Nature* 451:591–595.
26. Di Russo NV, Estrin DA, Martí MA, Roitberg AE (2012) pH-dependent conformational changes in proteins and their effect on experimental pK(a)s: The case of Nitrophorin 4. *PLOS Comput Biol* 8:e1002761.
27. Isom DG, et al. (2013) Protons as second messenger regulators of G protein signaling. *Mol Cell* 51:531–538.
28. Hirano T, et al. (2011) Conformational dynamics of wild-type Lys-48-linked diubiquitin in solution. *J Biol Chem* 286:37496–37502.
29. Lai MY, Zhang D, Laronde-Leblanc N, Fushman D (2012) Structural and biochemical studies of the open state of Lys48-linked diubiquitin. *Biochim Biophys Acta* 1823:2046–2056.
30. Gao J, et al. (2016) Cytosolic PINK1 promotes the targeting of ubiquitinated proteins to the aggresome-autophagy pathway during proteasomal stress. *Autophagy* 12:632–647.
31. Fiesel FC, et al. (2015) (Patho-)Physiological relevance of PINK1-dependent ubiquitin phosphorylation. *EMBO Rep* 16:1114–1130.
32. Matsuyama S, Reed JC (2000) Mitochondria-dependent apoptosis and cellular pH regulation. *Cell Death Differ* 7:1155–1165.
33. Raimondo JV, et al. (2016) Tight coupling of astrocyte pH dynamics to epileptiform activity revealed by genetically encoded pH sensors. *J Neurosci* 36:7002–7013.
34. Mabe H, Blomqvist P, Siesjö BK (1983) Intracellular pH in the brain following transient ischemia. *J Cereb Blood Flow Metab* 3:109–114.
35. Lagadic-Gossmann D, Huc L, Lecureur V (2004) Alterations of intracellular pH homeostasis in apoptosis: Origins and roles. *Cell Death Differ* 11:953–961.
36. Pickart CM, Raasi S (2005) Controlled synthesis of polyubiquitin chains. *Methods Enzymol* 399:21–36.
37. Liu Z, Tang C (2016) Ensemble structure description of Lys63-linked diubiquitin. *Data Brief* 7:81–88.
38. Schwieters CD, Kuszewski JJ, Tjandra N, Clore GM (2003) The Xplor-NIH NMR molecular structure determination package. *J Magn Reson* 160:65–73.
39. Müller BK, Zaychikov E, Bräuchle C, Lamb DC (2005) Pulsed interleaved excitation. *Biophys J* 89:3508–3522.
40. Homeyer N, Horn AH, Lanig H, Sticht H (2006) AMBER force-field parameters for phosphorylated amino acids in different protonation states: Phosphoserine, phosphothreonine, phosphotyrosine, and phosphohistidine. *J Mol Model* 12:281–289.
41. Liu Z, et al. (2012) Noncovalent dimerization of ubiquitin. *Angew Chem Int Ed Engl* 51:469–472.
42. Kalinin S, et al. (2012) A toolkit and benchmark study for FRET-restrained high-precision structural modeling. *Nat Methods* 9:1218–1225.
43. Delaglio F, et al. (1995) NMRPipe: A multidimensional spectral processing system based on UNIX pipes. *J Biomol NMR* 6:277–293.
44. Vranken WF, et al. (2005) The CCPN data model for NMR spectroscopy: Development of a software pipeline. *Proteins* 59:687–696.
45. Hansen MR, Mueller L, Pardi A (1998) Tunable alignment of macromolecules by filamentous phage yields dipolar coupling interactions. *Nat Struct Biol* 5:1065–1074.
46. Rücket M, Otting G (2000) Alignment of biological macromolecules in novel nonionic liquid crystalline media for NMR experiments. *J Am Chem Soc* 122:7793–7797.
47. Ottiger M, Delaglio F, Bax A (1998) Measurement of J and dipolar couplings from simplified two-dimensional NMR spectra. *J Magn Reson* 131:373–378.
48. Shen Y, Delaglio F, Cornilescu G, Bax A (2009) TALOS+: A hybrid method for predicting protein backbone torsion angles from NMR chemical shifts. *J Biomol NMR* 44:213–223.
49. Vuister GW, Bax A (1993) Quantitative J correlation: A new approach for measuring homonuclear three-bond J(H(N)H(alpha)) coupling constants in ^{15}N-enriched proteins. *J Am Chem Soc* 115:7772–7777.
50. Schwieters CD, Clore GM (2008) A pseudopotential for improving the packing of ellipsoidal protein structures determined from NMR data. *J Phys Chem B* 112:6070–6073.
51. Bermejo GA, Clore GM, Schwieters CD (2012) Smooth statistical torsion angle potential derived from a large conformational database via adaptive kernel density estimation improves the quality of NMR protein structures. *Protein Sci* 21:1824–1836.
52. Dolinsky TJ, Nielsen JE, McCammon JA, Baker NA (2004) PDB2PQR: An automated pipeline for the setup of Poisson–Boltzmann electrostatics calculations. *Nucleic Acids Res* 32:W665–W667.
53. Bonev BB, Chan WC, Bycroft BW, Roberts GC, Watts A (2000) Interaction of the lantibiotic nisin with mixed lipid bilayers: A ^{31}P and ^{2}H NMR study. *Biochemistry* 39:11425–11433.
54. Shaka AJ, Keeler J, Frenkiel T, Freeman R (1983) An improved sequence for broad band decoupling: WALTZ-16. *J Magn Reson* 52:335–338.
55. Lee NK, et al. (2005) Accurate FRET measurements within single diffusing biomolecules using alternating-laser excitation. *Biophys J* 88:2939–2953.
56. Gopich IV (2015) Accuracy of maximum likelihood estimates of a two-state model in single-molecule FRET. *J Chem Phys* 142:034110.
57. Burnham KP, Anderson DR (2004) Multimodel inference: Understanding AIC and BIC in model selection. *Sociol Methods Res* 33:261–304.
58. Schwarz G (1978) Estimating the dimension of a model. *Ann Stat* 6:461–464.
59. Akaike H (1974) A new look at the statistical model identification. *IEEE Trans Automat Contr* 19:716–723.
60. Vogelsang J, et al. (2008) A reducing and oxidizing system minimizes photobleaching and blinking of fluorescent dyes. *Angew Chem Int Ed Engl* 47:5465–5469.
61. Laskowski RA, Rullmannn JA, MacArthur MW, Kaptein R, Thornton JM (1996) AQUA and PROCHECK-NMR: Programs for checking the quality of protein structures solved by NMR. *J Biomol NMR* 8:477–486.
62. Hooft RW, Vriend G, Sander C, Abola EE (1996) Errors in protein structures. *Nature* 381:272.